UCRL-ID-137240

Flow Around a Complex Building: Comparisons Between Experimental and Modeled Results

R. Calhoun, S. Chan, F. Gouveia, R. Lee, J. Leone, J. Shinn and D. Stevens

November 22, 1999

U.S. Department of Energy

Lawrence
Livermore
National
Laboratory

DISCLAIMER

Work performed under the auspices of the U. S. Department of Energy by the University of California Lawrence Livermore National Laboratory under Contract W-7405-Eng-48.

Flow around a complex building: comparisons between experimental and modeled results

R. Calhoun, S. Chan, F. Gouveia, R. Lee, J. Leone, J. Shinn, and D. Stevens

November 22, 1999

1. INTRODUCTION

We compare the results of computer simulated flow fields around building 170 (B170) at Lawrence Livermore National Laboratory (LLNL) with field measurements. This is the first stage of a larger effort to assess the ability of computational fluid dynamics (CFD) models to predict atmospheric dispersion scenarios around building complexes. At this stage, the focus is on accurate simulation of the velocity field. Two types of simulations were performed: *predictive* and *post-experiment*. The purpose of the predictive runs was primarily to provide initial guidance for the planning of the experiment. By developing an approximate understanding of the major features of the flow field, we were able to more effectively deploy the sensors.

The post-experiment runs were performed for several reasons: 1) The largest amount of experimental data was available for slightly different wind directions than the directions used in the initial calculations. The predictive runs simulated three wind directions: 200, 225, and 250 degrees measured from true north. Although, the winds did blow generally from the southwest (typical summer conditions for this site), the most appropriate data available was for 210, 225, and 240 degrees. 2) We wanted to explore the sensitivity of the predictions to various levels of idealization that are by necessity a part of the modeling process. For example, what level of detail is required to accurately model the effect of the trees? How much architectural detail should be included in the model of the building? Figure 1 shows the level of idealization of the building for the predictive and post-experiment cases.

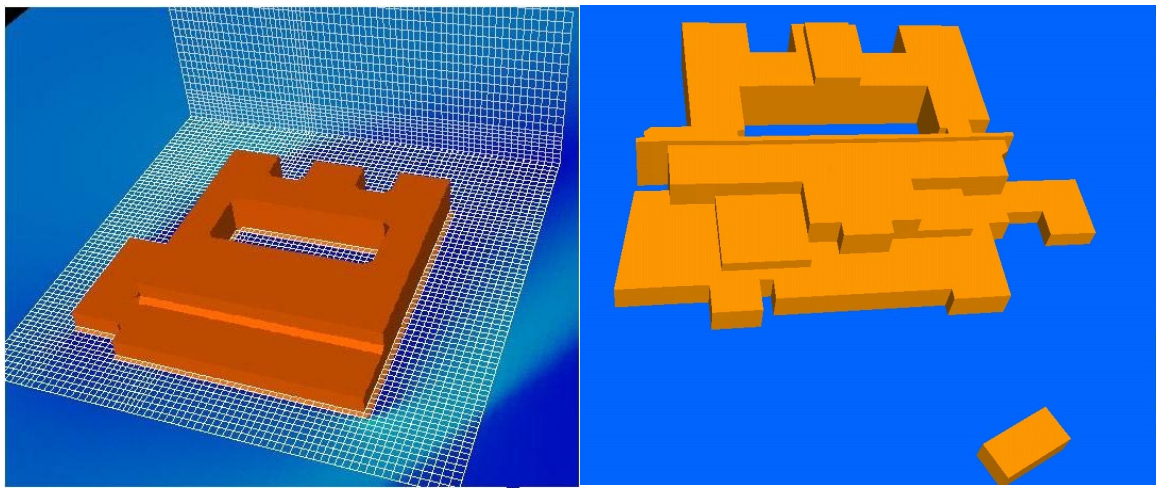

Figure 1. Building 170 models for the *predictive* (left) and *post-experiment* (top) runs. The northerly direction is oriented toward the top of the graphics.

In the following sections, we will discuss the model setup and solution techniques, the

experimental methods, and detailed comparisons of model versus experimental data.

2. MODEL SETUP AND NUMERICAL METHODOLGY

A. Problem Setup

Several important aspects of the simulation parameters are:

1) The flow was assumed neutral and no heat flux was imposed at the ground, representing cloudy or morning conditions. Consequently, only the experimental data which also represented neutral flow conditions was used in the following comparisons.
2) Canopy effects (trees) were modeled with the addition of a drag term in the momentum equations. In the predictive case, the canopy was modeled according to our conjecture that the major canopy effects were caused by line of Eucalyptus trees to the east (right) of the building. To test this hypothesis, we included more detailed canopy effects in the post-experiment runs. In Figure 2, the blue areas surrounding the building correspond with the locations and shapes of trees in the domain. In the post-experiment case, gaps between the Eucalyptus trees and the surronding ornamental trees were included in the model. In the vertical direction, the canopy is modeled as a two layered structure where a larger drag coefficient is assigned above the canopy base height and a lower drag is specified in the trunk area below the bulk of the limbs and leaves.

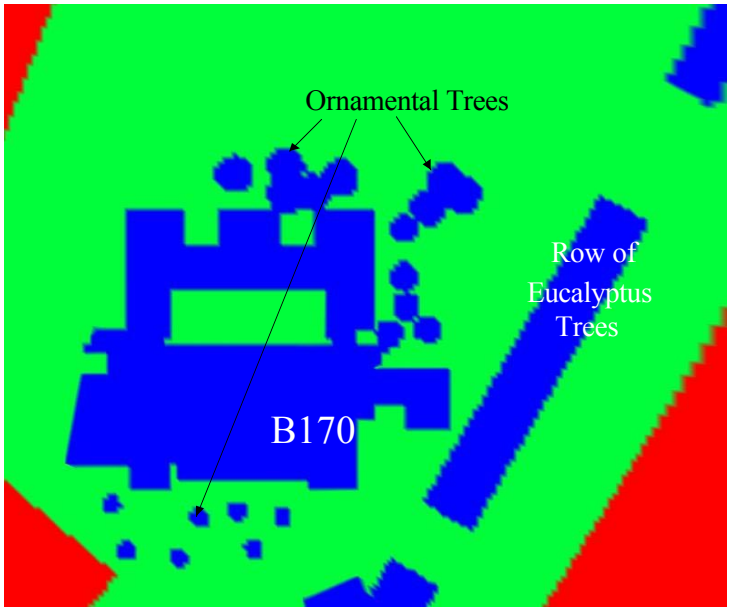

Figure 2. B170 tree locations. (Red areas locate major macadamized areas.)

3) The wind directions used in the predictive study were 200, 225, 250 degrees measured clockwise from true north (the prevailing winds at LLNL are from the southwest in the

summer). The wind directions in the post-experiment cases were redone to better match the gathered data: 210, 225, 240 degrees.

4) The incoming wind profile was modeled as logarithmic with a maximum of about 3 meters per second at the upwind height of 3 meters.
5) Approximately 1 million grid points were utilized for the predictive run and 2.5 million were used for the post-experiment run.

B. Summary of numerical methodology

The computational fluid dynamics code utilizes a finite element methodology (Chan, 1994) and has been adapted for use on massively parallel computer platforms (Stevens et al., 1999) via MPI (Message Passing Inteface). The simulations performed here used 128 processors of the ASCI Blue-Pacific machine. The computational domain spans 400 x 400 x 80 meters, where the smaller dimension is in the vertical direction. A variety of different turbulent closures have been implemented and are available in the massively parallel code (see, for example, Gresho and Chan, 1998). The results presented here are Reynolds averaged solutions (RANS) utilizing the similarity-k turbulence model. Simply by changing an input option, our code may also be utilized in large-eddy simulation (LES) mode, whereby some of the turbulence is explicitly resolved and only the subgrid turbulence is modeled. This is a more computationally expensive option since the resulting transient fields must be averaged to obtain results representative for the mean fields. It should be noted as well that if most of the turbulence is unresolvable on a numerical mesh, then the subgrid-scale model performs essentially as a RANS turbulence model.

3. FLOW EXPERIMENTAL AND DATA COLLECTION

A. Goals and experimental strategies

The goal of the experiment was to provide air-flow data around the exterior of the building 170 that could be used to validate the CFD models under development. One strategy was to make an estimate of the flow field using an overly simplified form of the CFD model, and to use these results to determine placement locations for the wind sensors. In another strategy to reduce the number of sensors required, the wind speed was normalized to wind speed observed at an upwind reference station. This allowed measurements to be taken at different times with the same wind sensors. By using 8 sonic anemometers in a movable array, the normalization provided the equivalent of 54 sonic anemometers operating simultaneously at a fixed height of 2.6 m.

The upwind reference station was an energy budget system that measured wind speed and direction as well as the sensible heat flux to the ground surface. Additional wind information was provided by a weather station on top of the building, a permanent weather tower with wind measured at 10-m and 40-m heights, and an acoustic sounder (sodar) on top of the building. The sodar provided winds averaged over 50-m layers up to the 250-m height. Because the data is not yet processed, we do not use the sodar data in this report.

Because of normal variability in wind data, criteria were set up to determine which data would be rejected and the remainder used for model validation. The long-term weather records from the permanent weather tower showed that at the 10-m height the median wind speed is 2.6 m/s and the 95th-percentile is 6 m/s in annually-compiled data (i.e., 5% of the windspeeds are greater than 6 m/s). During the summer months at LLNL, the prevalent wind is from the southwest (SW) with recurrence frequencies more than 60%. These recurrence frequencies reduce to about 20% by November. The first criterion was that the wind data should be retained when the wind direction was approximately from the SW; in practice all data was retained from the quadrant 195° to 285°. The second criterion was that with the above definition of "upwind", the wind data should be retained when the wind speed exceeded 2 m/s and the atmospheric stability conditions were neutral at the energy budget reference station. The latter criteria provided assurance that the Monin-Obukhov length-scale would be practically infinite for the inflow air to B170.

It was decided to acquire the data in one-second polls and immediately process that into 10-minute averages and standard deviations. The 10-minute averages were to represent, in some time averaged sense, meteorologically-relevant mean variations of the winds at the measurement locations. The sonic anemometers (Handar, model 425) measured horizontal wind components only and were programmed to provide a pulse-type of square wave output for the digital channels in the data acquisition systems (Campbell Scientific, model CR-10). These data loggers with 2 sonic anemometers each were normally able to operate in the averaging mode for 5-10 days without overwriting the memory buffers. But in a special wind variability study the sonic anemometers were operated continuously at one-second polls without preprocessing to average states. In these special cases the data loggers would overwrite the memory buffers in about two hours.

Quality assurance was provided by a quality control procedure of inspection of sonic anemometer performance in a slow-speed wind tunnel (1-2.5 m/s), and by the periodic quality control normalization of placing all sonic anemometers at the same height and approximate location as the upwind energy budget station over 3 to 5 days (400 to 700 10-minute periods). These quality assurance procedures to compare resolved speed and direction produced speed component measurement accuracy within 3% and with absolute accuracy and resolution of 0.1 m/s. The only problems encountered were with one anemometer that proved to have a non-trivial calibration zero offset, two anemometers that required output span adjustments, and one failure due to corrosion within the sonic anemometer case. Since a spare sonic anemometer was retained, there was only a trivial amount of data lost.

B. Experimental Data Set

Sonic anemometers were deployed eight at a time in arrays denoted as "stations". Each station was allowed to acquire data for approximately one week. Reduction of the data in a spreadsheet allowed the data to be sorted according to the retention criteria, converted from conventional wind direction and speed to wind speed components and then sorted by 10-min upwind wind direction. At this stage the component speed data were graphed according to upwind wind direction and inspected. In this manner wind speed components were seen to undergo a smooth transition in a continuous curve along the independent variable of upwind wind direction. This analysis showed that each 10-min period was representative and repeatable, and definitely not a random occurrence. Then data were combined into 5-degree bins to provide smoothing. These speed components comprise the data set for 53 locations (one location was lost due to instrument failure). In addition, the same locations provided standard deviations of the wind direction for optional determination of turbulence intensity or approximate turbulent kinetic energy. A

special study was undertaken to obtain a minimum of wind variability data for six of the 54 locations. In that study, 6 sonic anemometers were operated for one week with no 10-minute summary, so that the memory buffers retained the one-second data but filled up in about two hours. Several 2-hour periods that met the criteria were retained. From these, data collected for one hour during the most persistent SW wind was retained as a benchmark data set.

4. MODEL - EXPERIMENT COMPARISONS

In the following, we present both graphical and numerical comparisons between the experimental data and model results. The simplest and most illuminating method of comparison is to overlap experimental and model vectors at the sensor locations. It is more challenging to interpret numerical comparisons because one cannot see and easily evaluate the cause and importance of errors. For example, near a corner of the building there may be strong gradients and a recirculation zone where strong positive velocities exist near to small negative velocities. Because the sensor locations may potentially contain an error on the order of 1 meter, even a "perfect" model solution may not perform well with some numerical metrics. In these cases, it is important to understand if the *mean dynamics* are well represented. Are the mean structures present with approximately the correct magnitudes and directions of rotation? We will provide this type of analysis when needed to support numerical comparisons provided below.

A. Numerical measures of comparison

We compare magnitudes of the velocity vectors with *mean absolute deviations.* These are defined as follows:

$$mDev = \frac{1}{N}\sum \left| U_{\text{mod}} - U_{\text{exp}} \right|$$

In the above formula, N represents the number of sensor locations being compared and U represents the magnitudes of the experiment or the model depending on the subscript. The above formula will be applied globally and by regions to the domain. The regions are defined in Figure 3 as: 'north', 'south', and 'east'. There is not enough data to define a separate 'west' region.

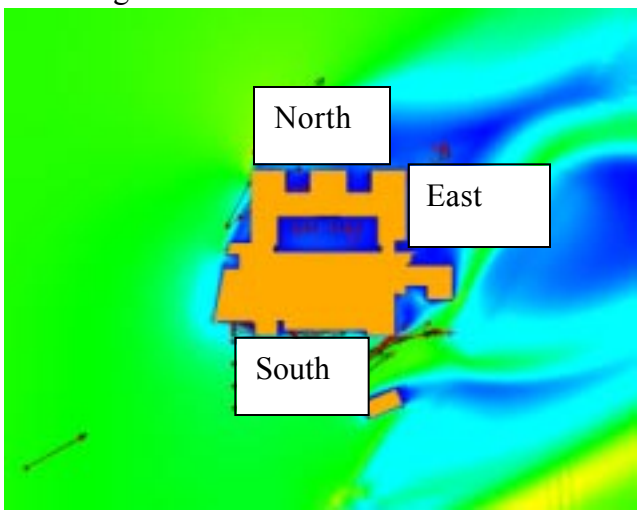

Figure 3. Regions for numerical comparisons.

Angles will be compared by using *scaled average angle differences*, defined as follows:

$$SAA = \frac{\left(\sum |U_i| \phi_i\right)}{\left(N \overline{|U_i|}\right)}$$

Where ϕ_i above is the angle between measured and modeled velocity vectors, and N is the number of samples being averaged over. The angle difference is scaled by the magnitude of the modeled velocity vector $|U_i|$ and then normalized by the average of the magnitudes over the sample space. The purpose behind scaling the angles by the magnitudes is to weight the angles of the larger vectors more strongly. The justification for this is twofold: 1) The errors associated with the small vectors are relatively larger due to limitations with the anemometers, and 2) For transport purposes, angles associated with smaller vectors are less important than angles of larger vectors.

B. Predictive Case - 225 degree wind direction

Figure 4 shows sensor locations and the corresponding wind vectors for both the experimental data and the predictive model for 225 degree winds. The white vectors are from the experiment and the black are modeled vectors. The bulk of the sensor locations are on the south side of the building and in general the agreement here both in terms of velocity magnitude and direction is quite good. The major challenges remaining for this model in this area are to correctly capture the turning angle of the vectors as wind moves around the southeast corner of the building. The model predicted a stronger turning around the corner than is observed in the experiment. We hypothesized that the over-turning of the modeled winds were a result of modeling the Eucalyptus trees as a single, unbroken canopy region. In fact, there is a reasonably large gap in the treeline in several locations, one of them located near the southeast corner. Therefore, in the post-experiment runs, we test this hypothesis by including the gap in the trees. Notice that on the north and east side of the building, the mean dynamics are well represented. The direction of the recirculation on the east side is correct and the vectors on the northside agree reasonably well. The model prediction for the courtyard was a helical pattern with flow exiting the east-north corner of the courtyard. A conclusive evaluation of the dynamics for the courtyard is not possible with the data available. It is clear, however, that the experimental vectors are larger in parts of the courtyard than the model anticipated. The discrepancy may in part be attributable to the ornamental vine-supporting structure in the center of the courtyard which was not included in the simulation.

Numerical comparison.

The following table is distilled from a spreadsheet comparing modeled and experimental data. The middle column describes how the angles compare and the last column compares magnitudes scaled by the magnitude of the ambient vector (the upstream wind vector). Notice that the angles (in degrees) compare well for the global, south, and north regions. The larger error in the angles on the east side is due to the difficulty of precisely modeling the *position* of essentially correct dynamics. We elaborate on this discussion for the 240 degree case below. The errors in the magnitudes are less for the south side and highest, relative to the ambient, near the north side.

Case	*SAA*	*Mdev/ambient*
Global	9.1	0.13
South	6.2	0.09
North	5.7	0.23
East	29	0.15

C. Post-experiment case - 225 degree wind direction

Notice in this case (Figure 5) that channeling between the gaps in the trees has developed and that this has improved the angles on the south side of the building near the eastern corner. The recirculation on the east side displays the same counter clockwise rotating mean circulation that is found in the experimental data. The northern side shows a correct clockwise rotation although experimental results show a recirulation tighter to the building than the model results. Figures 6, 7, and 8 show magnified views of each of the regions. Red vectors are the experimental values, black are the model. Surprising large values for the experimental results exist near the eastern side of the courtyard. These are likely a result of additional ornamental structures in the courtyard. Higher than ambient velocities are present around the northwest corner of the building, and the model correctly predicts these (although a larger value is predicted than found in the experiment: 3.5 versus 3.1 m/s). A higher than ambient jet is not found near the southeast corner of the building (for either model or experiment at the sensor locations). Figure 9 shows calculated pressure values on the building surface. Notice that there are potentially significant pressure differences between various levels of the building. The intakes for this building are near the second level. A pressure difference of about 3 Pascals exists across the building in the west-east direction. (All pressures are in Pascals.)

Numerical comparison

As in the predictive case, the south region shows good overall accuracy in both angle and magnitudes. As before, positioning of the north side recirculation is somewhat more difficult to capture. Note that the overall level of accuracy is comparable to the predictive case *at the current positions of the sensors.* It is likely that improvements in the post-experiment model run may be found at other locations; for example, at higher vertical locations or near the gaps of the trees.

Case	*SAA*	*Mdev/ambient*
Global	11.4	0.15
South	5.1	0.13
North	21.3	0.37
East	24	0.11

D. Post-experiment case - 210 degree wind direction

Figures 10, 11, and 12 compare vectors for the 210 degree case. As in the previous case, the model agrees well with the experiment on the south side. The east side recirculation is nearly as accurate, capturing reasonably well the corrrect mean circulation and approximate location. The challenge for this wind direction is on the north side. Both model and experiment find similar types of circulations, but the close proximity of very small recirculation values and nearly ambient velocities means that a small positioning error causes a large error in the vectors. The experiment does not find higher than ambient velocities near the northwest corner. The model does predict stronger than ambient velocities, but uncertainty in sensor location may be partially responsible. Near the southeast corner the experiment does find slightly higher than ambient wind speeds. Peak model values at the sensor locations near the southeast corner are close, nearly reaching the ambient level. Figure 13 shows pressure on the building, as in previous cases, there is roughly a three pascal difference in pressure between the west and east sides of the building. Relatively low values of pressure exist near the northwest corner.

Numerical comparison.

Case	***SAA***	***Mdev/ambient***
Global	10.6	0.16
South	3.3	0.16
North	34.1	0.27
East	18.7	0.13

E. Post-experiment case - 240 degree wind direction

Figures 14, 15, 16, and 17 allow analysis of 240 degree winds. In this case, the south side has generally good agreement, although there is a tendency for the model to exaggerate the turning effect of the building. For the north side, the model does better than in the previous case. Some discrepancies exist on the east side. A magnification of this area with surrounding model vectors in white (red is experiment and black is model at sensor location as in previous cases) shows that there is a mean eddy with the same direction in both the experiment and the model. However, the eddy in the experiment is larger and shifted farther to the south by about a fourth of the building's width. Therefore, even in this area where agreement is not on par with other regions, both the model and the experiment agree that there will be an area on the east side of the building which will experience westerly flowing winds. The winds in the courtyard are more nearly matched by the model vectors, perhaps because the ornamental features obstruct the flow along the line of sensors to a lesser degree. The two sensor locations along the west side of the building would appear to indicate that the model solution overextends the turning effect of the building (farther out into the flow field). Interestingly, for this wind direction, the experiment does not show a higher than ambient jet near either the northwest or southeast corners of the building. Model results, however, predict a higher than ambient jet around the northwest corner.

Numerical comparison.

Case	*SAA*	*Mdev/ambient*
Global	12.4	0.15
South	7.4	0.15
North	10.6	0.24
East	51	0.18

5. CONCLUSIONS

We have compared model versus experimental mean wind vectors for several wind directions. The model solution generally captures the mean dynamics of the flow field, and errors, when significant, can usually be at least partially attributed to differences in phase. However, the experiment has illuminated several areas where the model solution might be improved. Especially challenging are regions of the flow where large velocities are near small recirculations; although in these cases, uncertainty in the location of the sensors may be partially responsible for discrepancies. In addition, perturbations (caused by the building) in the angle of the vectors (relative to ambient winds) tend to attenuate more rapidly away from the building than the model predicts. The numerical metrics corroborate the impressions gained by inspection of the vector fields; i.e., that most of the discrepancies between the modeled and experimental wind fields are small relative to the ambient winds.

When considering the inherent level of uncertainty in atmospheric flows of this kind, the overall agreement between the modeled and experimental fields is remarkable. Accurately capturing the dynamics is a key first step towards better understanding dispersion scenarios. The next step is to evaluate which aspects of the flow field are most important for dispersion, and therefore which errors should be most strongly minimized. In addition, we have gathered high frequency anemometer data (sampled at a higher rate). This data is being analysed to gain insights into turbulent structures which exist behind buildings. High resolution LES results will be obtained to study the transient features of the flow.

6. REFERENCES

Gresho, P., and Chan, S., 1998, Projection 2 goes turbulent - and fully implicit, *Int. J. Comp. Fluid Dyn*, **9**, 249-272.

Chan, S., 1994, An improved three-dimensional heavy-gas dispersion model: User's Manual, UCRL-MA-116567 Rev. 1, Lawrence Livermore National Laboratory.

Stevens, D., Almgren, A., Bell, J., Beckner, V., and Rendleman, C., 1999, Small scale processes and entrainment in a stratocumulus marine boundary layer, *J. of the Atmos. Sci.,* In Press.

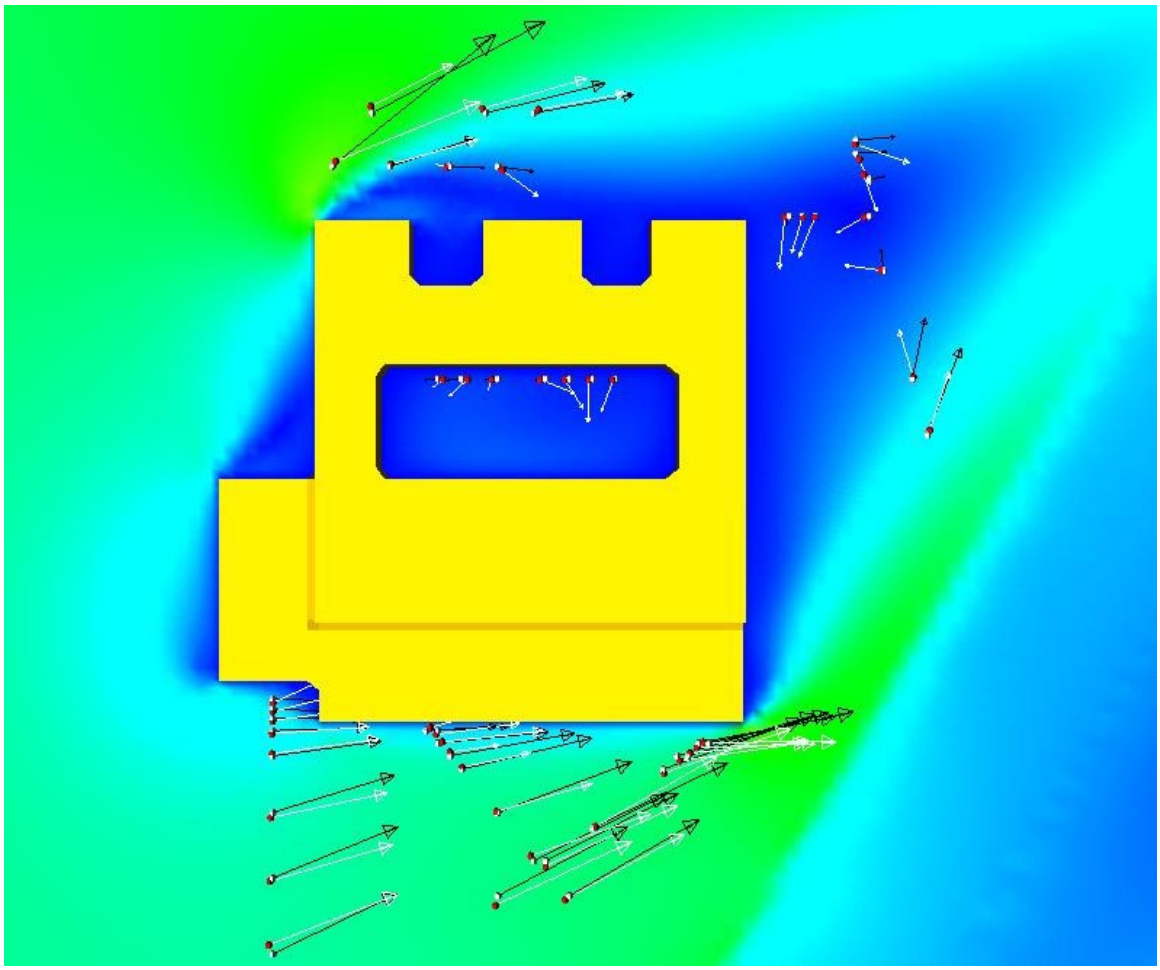

Figure 4. Model and experimental vectors for predictive case - 225 degree winds. White vectors are experimental data and black are model data.

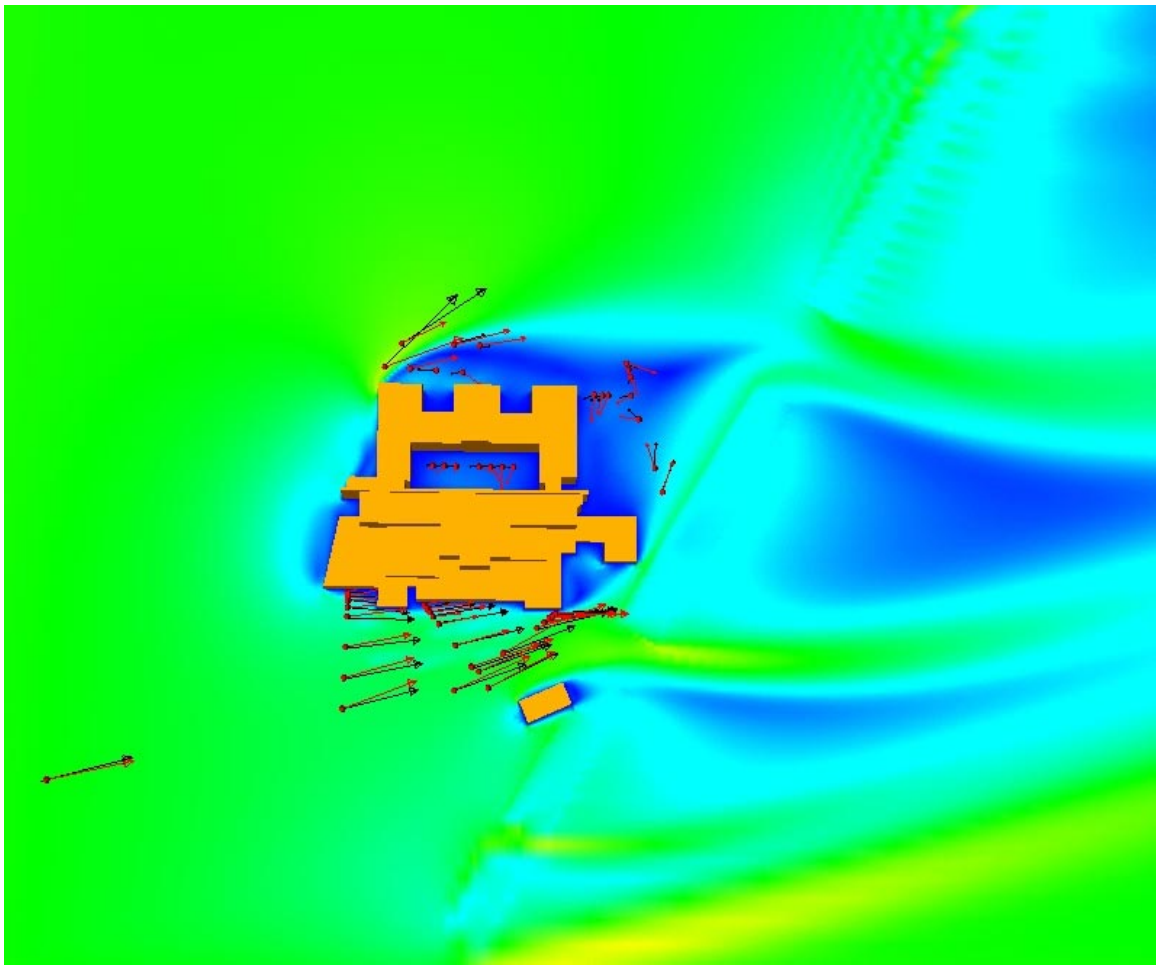

Figure 5. Model and experimental vectors for post-experiment case - 225 degree winds. Red vectors are experimental data, and black vectors are model data.

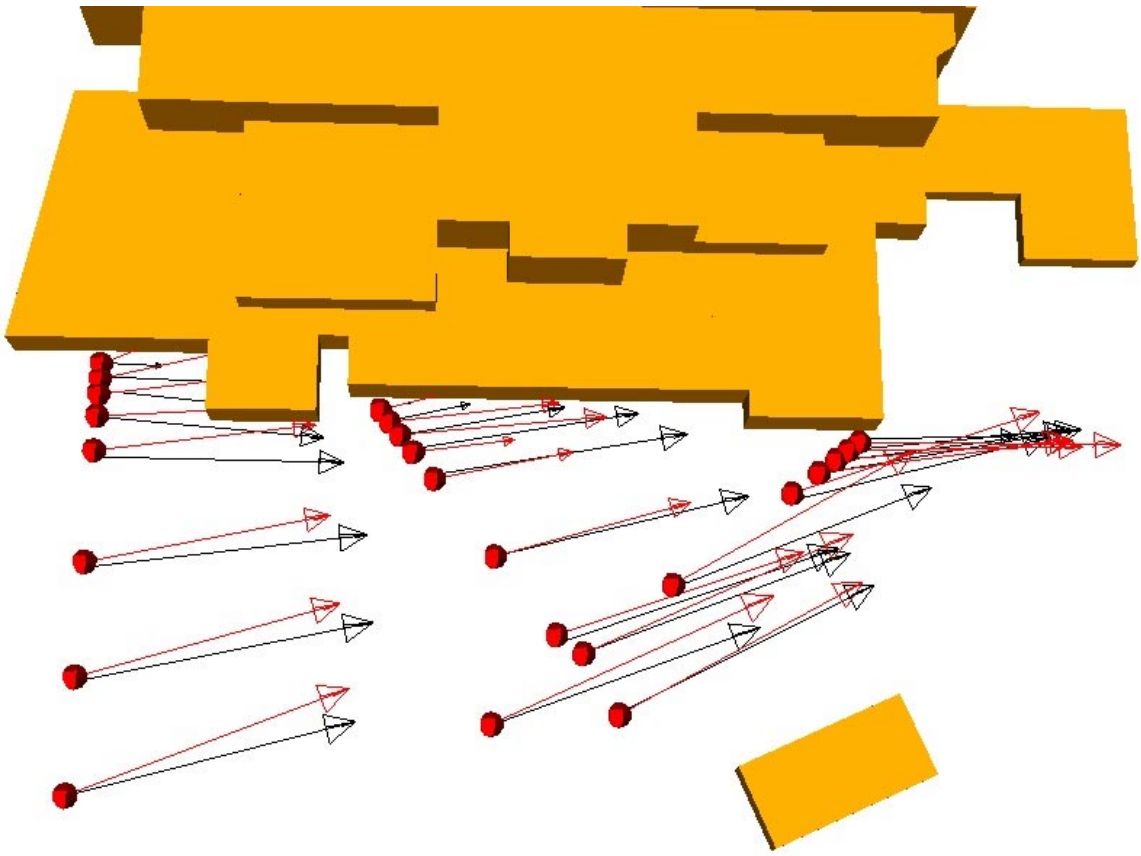

Figure 6. Model and experimental vectors for post-experiment case - 225 degree winds (south side). Red vectors are experimental data, and black vectors are model data.

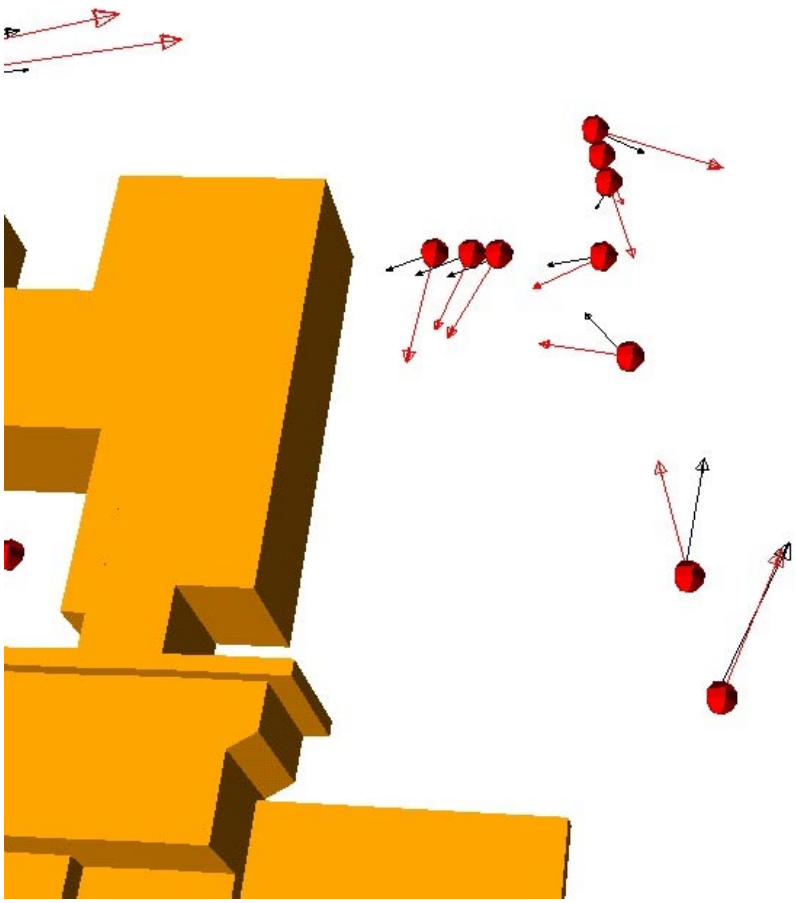

Figure 7. Model and experimental vectors for post-experiment case - 225 degree winds (east side). Red vectors are experimental data, and black vectors are model data.

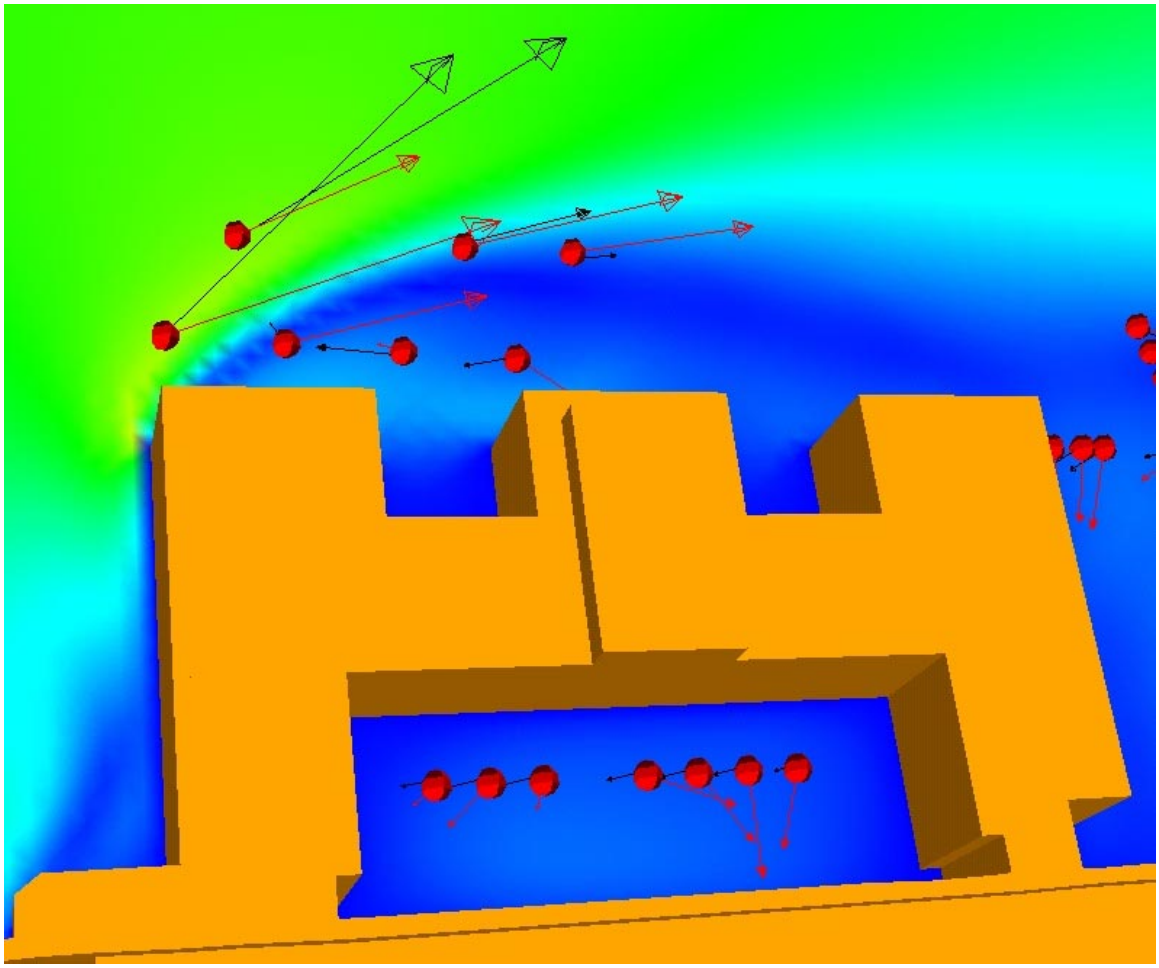

Figure 8. Model and experimental vectors for post-experiment case - 225 degree winds (north side). Red vectors are experimental data, and black vectors are model data.

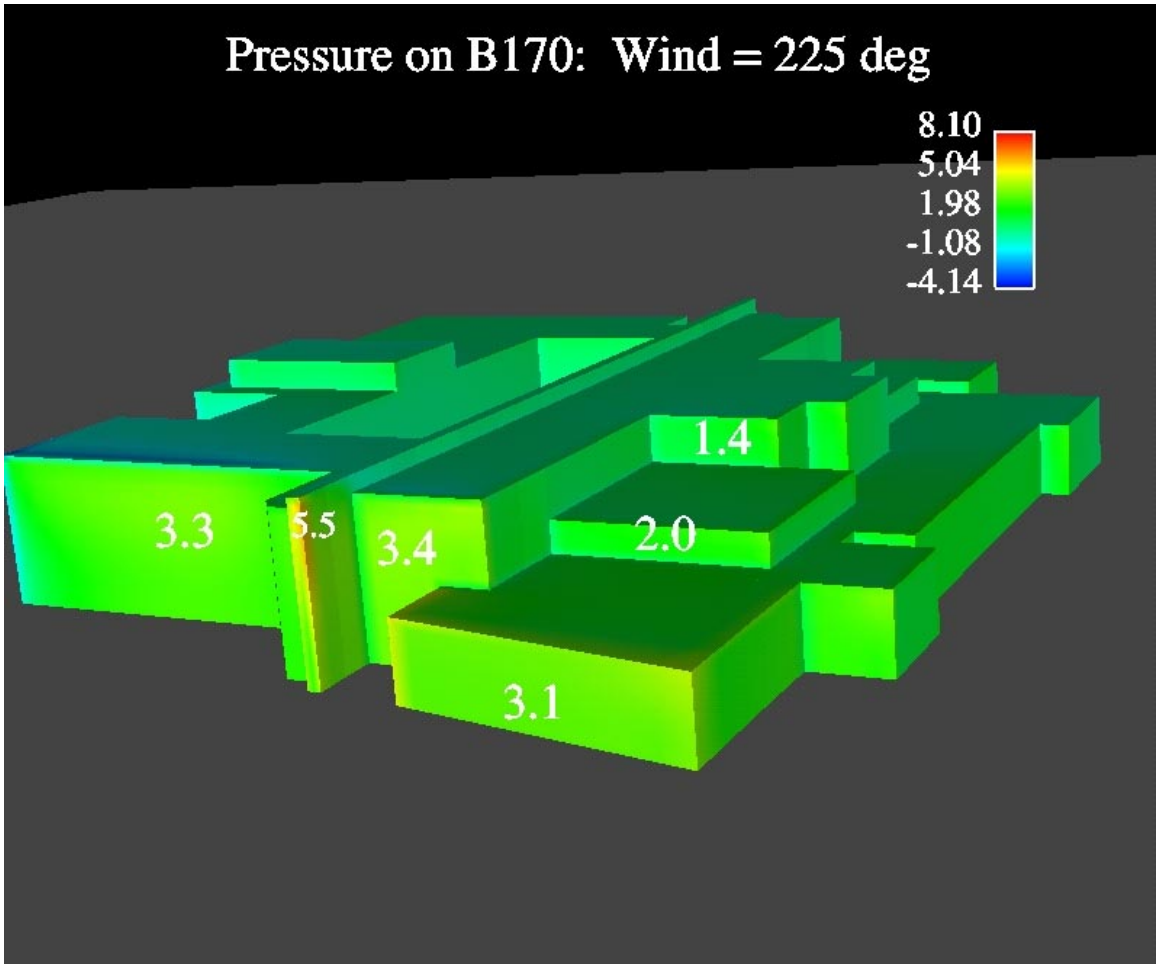

Figure 9. Pressure (in Pascals) for post-experiment case - 225 degree winds.

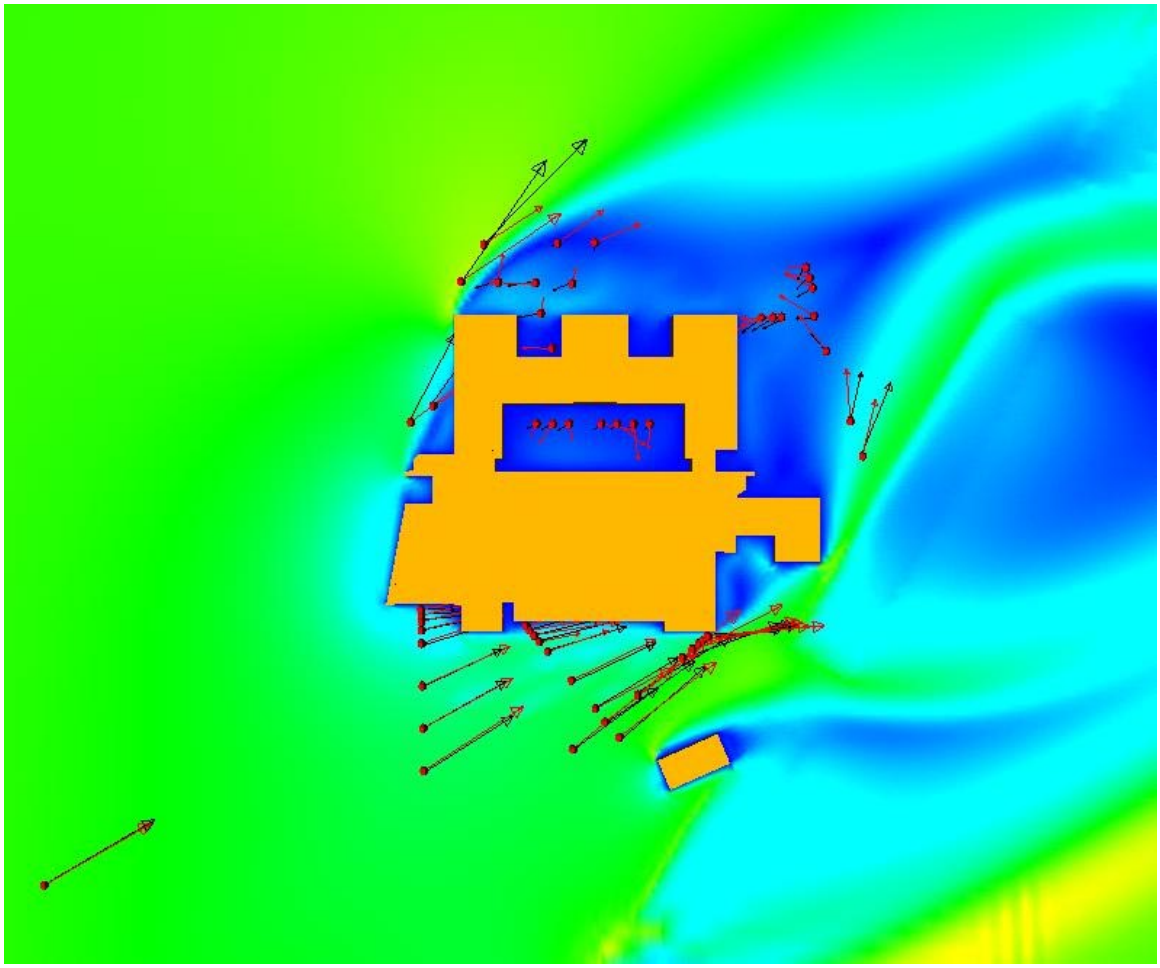

Figure 10. Model and experimental vectors for post-experiment case - 210 degree winds. Red vectors are experimental data, and black vectors are model data.

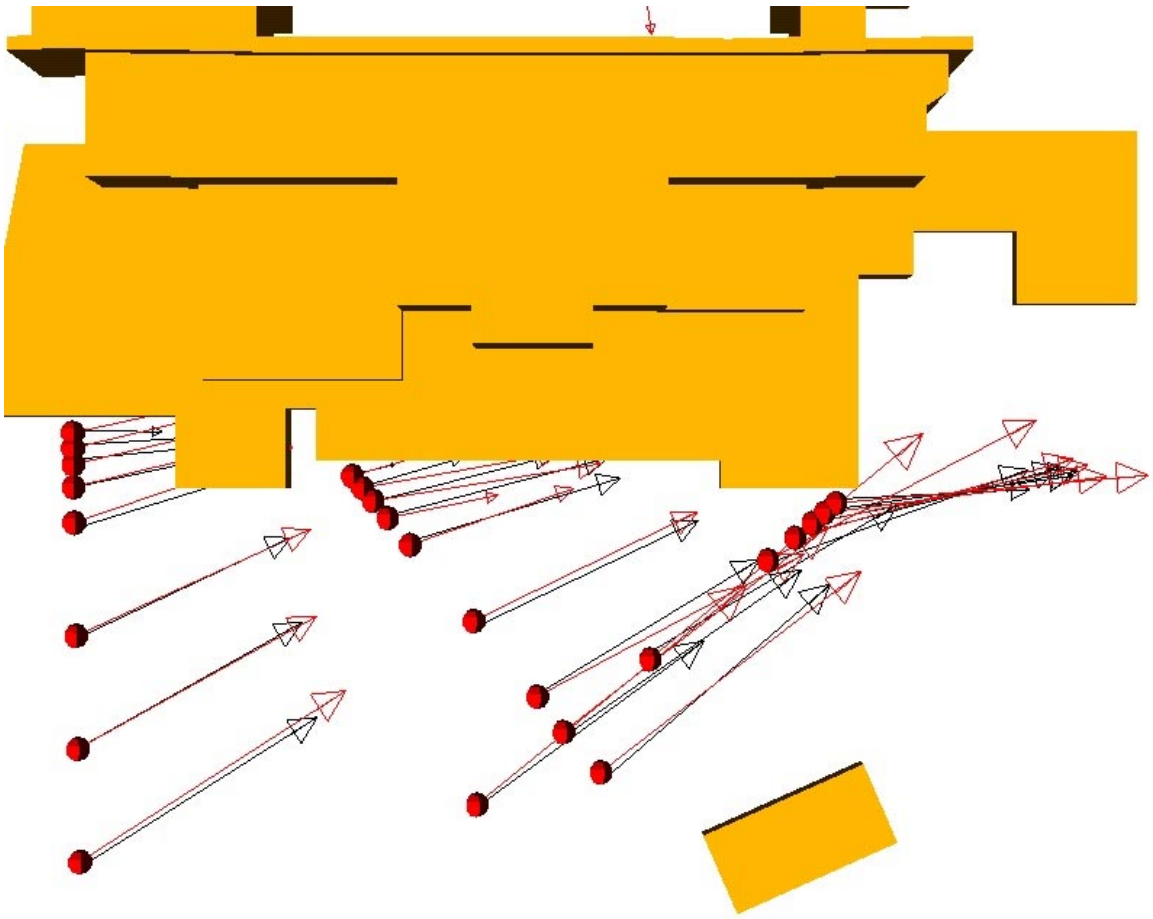

Figure 11. Model and experimental vectors for post-experiment case - 210 degree winds (south side). Red vectors are experimental data, and black vectors are model data.

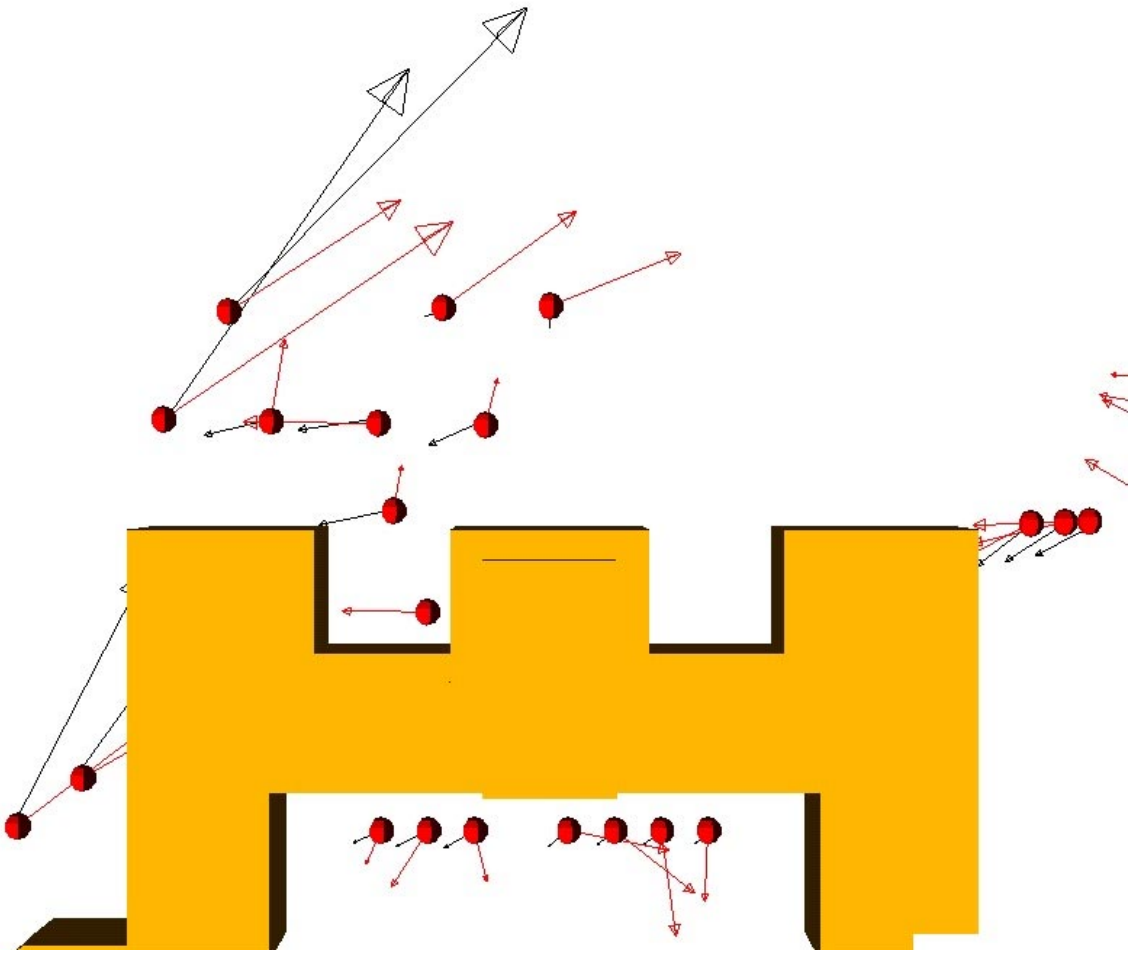

Figure 12. Model and experimental vectors for post-experiment case - 210 degree winds (north side). Red vectors are experimental data, and black vectors are model data.

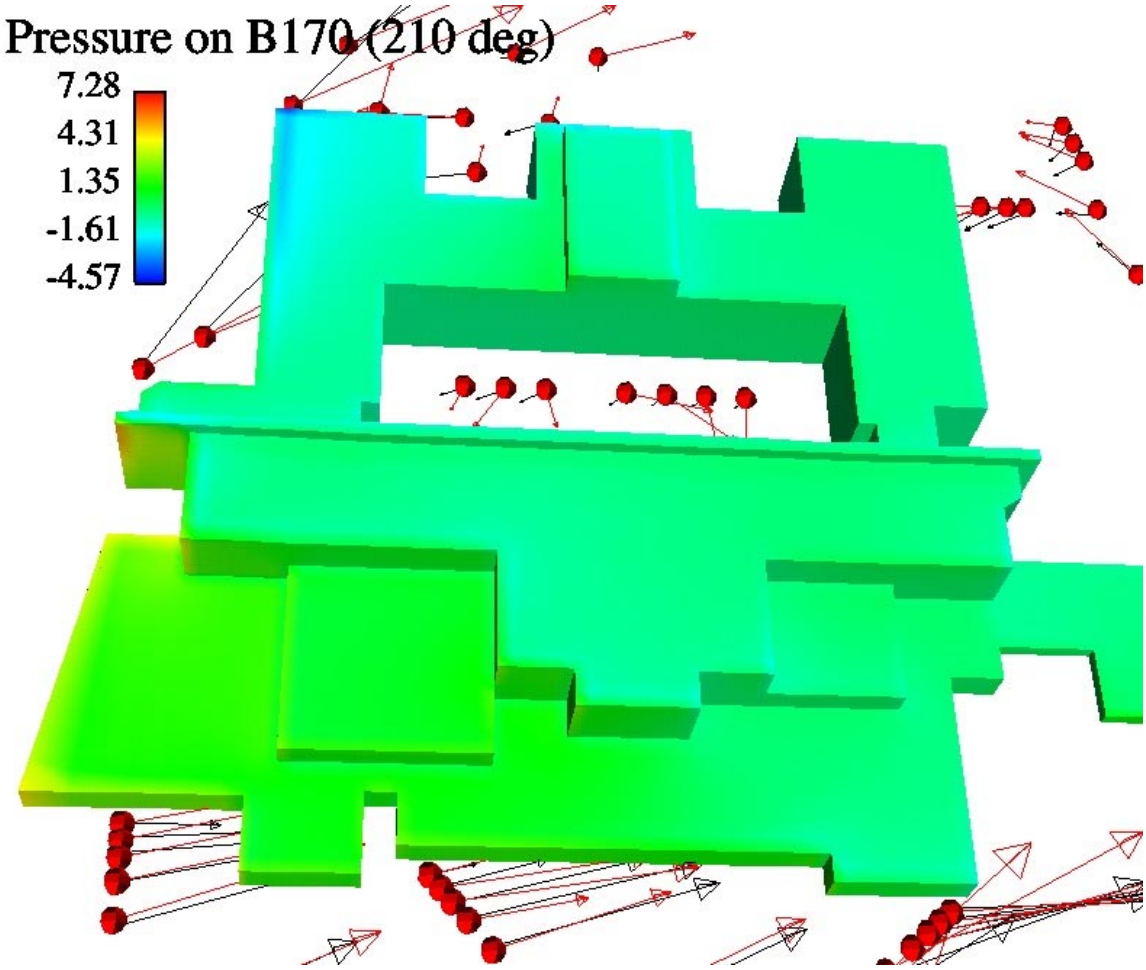

Figure 13. Pressure (in Pascals) for post-experiment case - 210 degree winds.

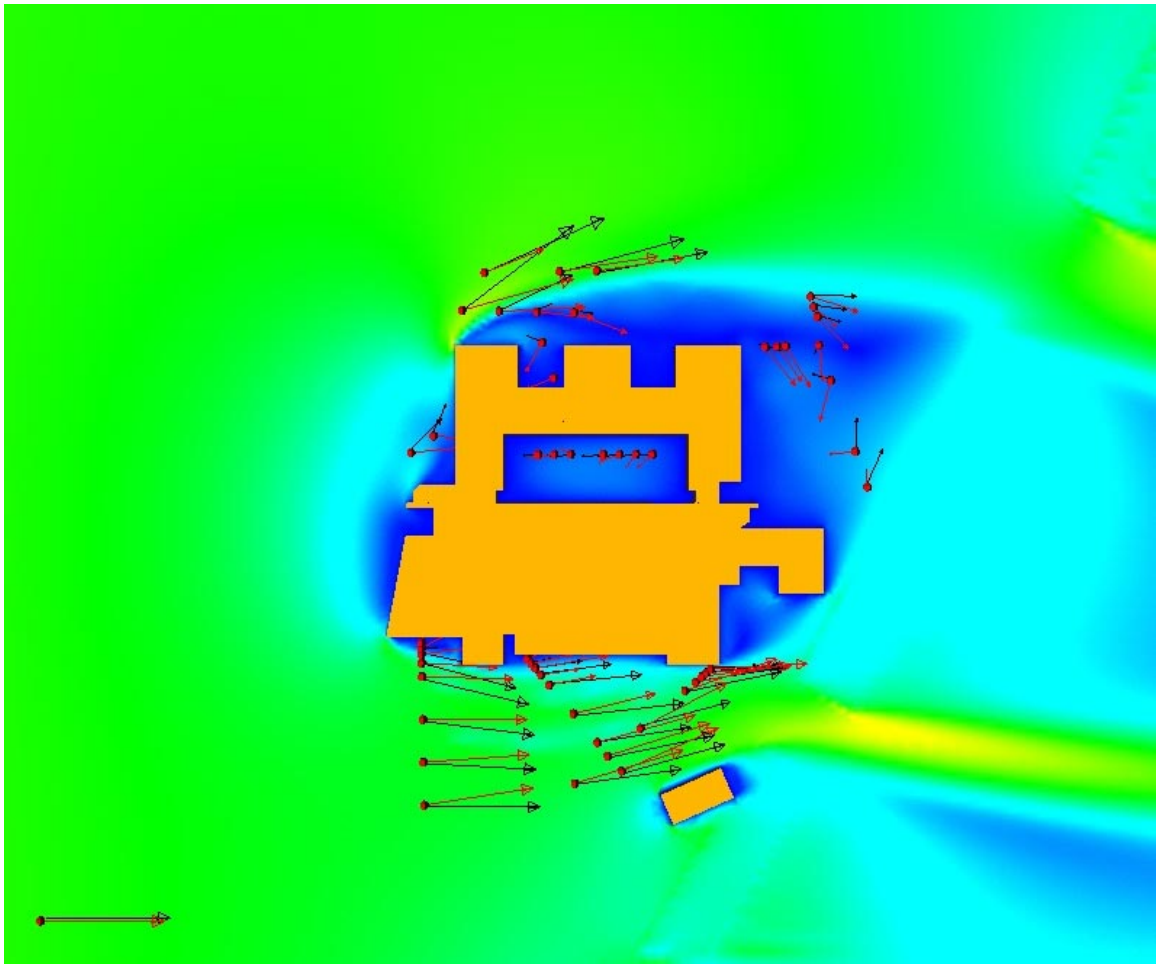

Figure 14. Model and experimental vectors for post-experiment case - 240 degree winds. Red vectors are experimental data, and black vectors are model data.

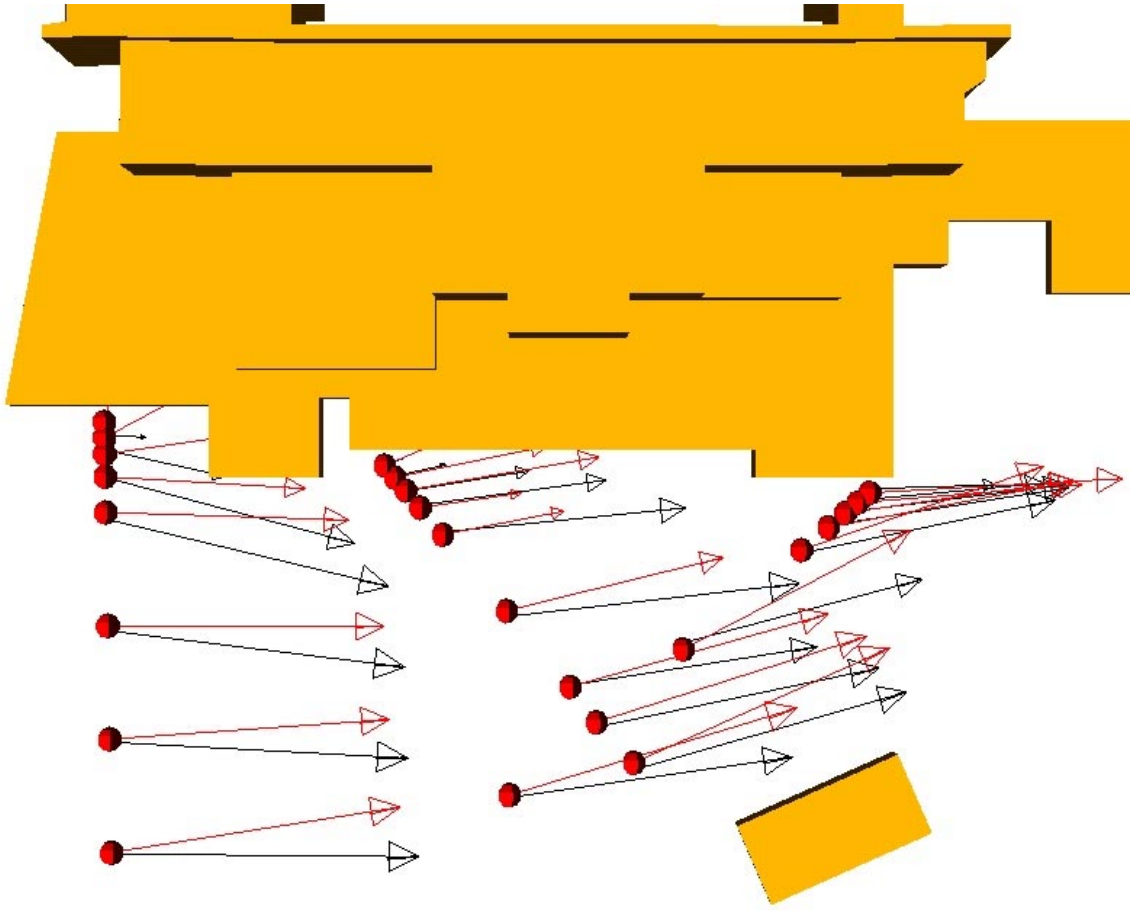

Figure 15. Model and experimental vectors for post-experiment case - 240 degree winds. Red vectors are experimental data, and black vectors are model data.

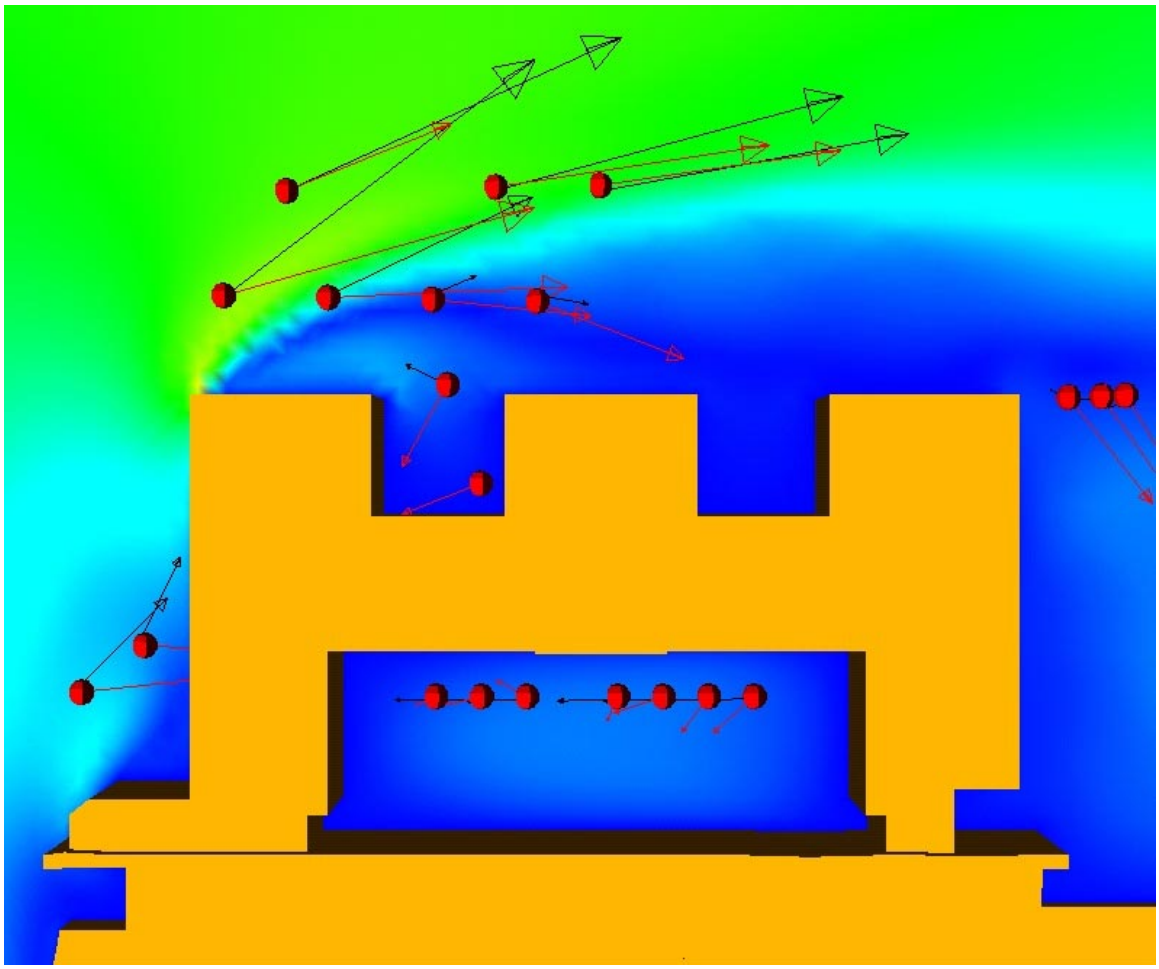

Figure 16. Model and experimental vectors for post-experiment case - 240 degree winds (north side). Red vectors are experimental data, and black vectors are model data.

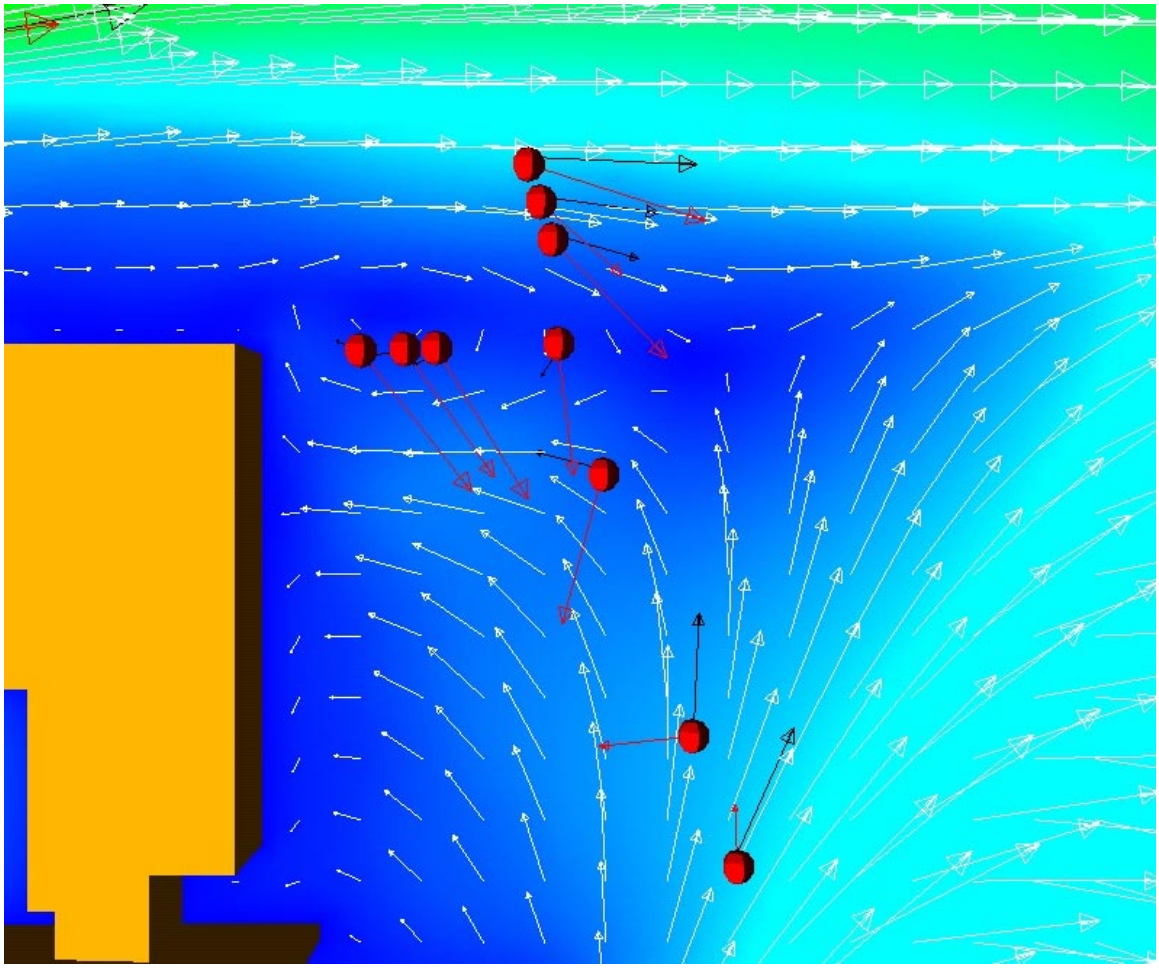

Figure 17. Model and experimental vectors for post-experiment case - 240 degree winds (east side). Red vectors are experimental data, black vectors are model data at sensor locations, and white vectors show model data for the surrounding area.